Memristor models for chaotic neural circuits

WCCI 2012 IEEE World Congress on Computational Intelligence
June, 10-15, 2012 - Brisbane, Australia IJCNN

Memristor models for chaotic neural circuits

F. Corinto
Department of Electronics
Politecnico di Torino
Corso Duca degli Abruzzi 24
Torino 10129, Italy
Email: fernando.corinto@polito.it

A. Ascoli
Department of Electronics
Politecnico di Torino
Corso Duca degli Abruzzi 24
Torino 10129, Italy
Email: alon.ascoli@polito.it

M. Gilli
Department of Electronics
Politecnico di Torino
Corso Duca degli Abruzzi 24
Torino 10129, Italy
Email: marco.gilli@polito.it

***Abstract*—Chaotic neural networks are able to reproduce chaotic dynamics observable in the brain of various living beings. As a result, study of the dynamical properties of such networks may pave the way towards a better understanding of the memory rules of the brain. In this paper a simple neural circuit employing a theoretical memristive synapse with symmetric charge-flux nonlinearity is found to behave chaotically. After presentation of a novel boundary-condition based model for real memristor nano-structures, conditions under which a suitable arrangement of such nano-structures is dynamically equivalent to the theoretical memristor are derived and validated.**

I. Introduction

The development of more and more sophisticated neural networks, capable to emulate increasingly complex cognitive functions, may guide researchers towards a better understanding of the way the brain works. A number of electrophysiological experiments carried out on various animals have recently revealed the chaotic dynamics experienced by ensembles of neurons. As a result, the study of the dynamical properties of chaotic neural networks [1] may lead us to gain a deeper insight into the associative memory dynamics [2] and the pattern recognition mechanisms [3] of the brain. Novel neural networks use the memory-resistor [4] to emulate the behavior of a biological synapse. As the ionic flow through a synapse finely modulates its weight, so the history of the voltage across the memory-resistor enables the plasticity of its conductance. The recent discovery of memristor behavior at the nano-scale is ascribed to Hewlett-Packard [5]. The lack of published experimental data in literature complicates the attempts to define reliable mathematical models for memristor nano-structures. However the derivation of such models is a necessary step towards the development of memristor-based chaotic neural networks. This paper first introduces a chaotic neural circuit [6] employing a theoretical memristor with odd-symmetric charge-flux nonlinearity [7]. Then, after a short presentation of a novel, simple, general and accurate boundary condition-based model for practical memristor nano-structures [8], an analytical treatment providing necessary and sufficient conditions under which a suitable arrangement of such nano-structures implements the above mentioned theoretical memristor, is provided. Such conditions are finally tested through numerical simulations on the variant of the chaotic neural circuit using the practical nano-structure combination in place of the theoretical memristor. Regarding the structure of this manuscript, Section II presents the original chaotic neural circuit, Section III revisits a number of models for memristor nano-structures. Section IV introduces the proposed boundary condition-based model, while Section V derives conditions under which such model exhibits a single-valued charge-flux relation. Under these conditions Section VI conceives appropriate memristor combinations with dynamical behavior equivalent to the theoretical memristor. Such dynamical equivalence is validated in Section VII. Finally Section VIII outlines the conclusions.

II. Chaotic neural circuit with theoretical memristor

The authors from [6] studied the complex dynamics of a memristor-based neural circuit. The circuit, shown in Figure 1, is a modified version of Chua's canonical oscillator, originally presented in Figure 7 of [7]. The modification consists in the replacement of Chua's diode with an active device made up of the parallel between a passive memristor and a negative conductance (G_{N2} in Figure 1). Further, the authors in [6] added a parasitic conductance in series with the inductor.

Referring to the symbols reported in Figure 1, application of Circuit Theory Laws to the oscillator yields its equations. In line with the assumptions done in [7], memristor m is flux-controlled and exhibits the following theoretical piece-wise linear (PWL) monotone-increasing odd-symmetric charge-flux characteristic:

$$q(\varphi) = b\,\varphi + \frac{a-b}{2}\left(|\varphi+1| - |\varphi-1|\right), \tag{1}$$

where q denotes the charge through the memristor, while a and b denote the nonlinearity parameters, whose sign is positive due to the passive nature of the device. This passivity implies the necessity to add a suitably-negative conductance in parallel with the memristor so as to obtain a locally-active device, i.e. a device characterized by a q-φ nonlinearity with a negative slope either on the central segment or on the two outer segments. This is an essential requirement for the occurrence of chaotic behavior in an autonomous dynamical system [9].

The memory-conductance of a memristor is defined as [4]

$$W(\varphi) = \frac{dq(\varphi)}{d\varphi}.$$

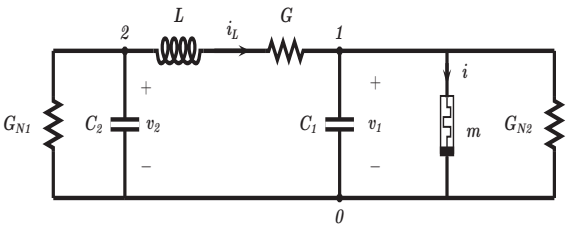

Fig. 1. Variant of Chua's canonical oscillator where Chua's diode is replaced with a locally-active device comprising a theoretical memristor m with symmetric q-φ nonlinearity in parallel with negative conductance G_{N2}.

Thus, flux differentiating (1), memristor m exhibits the following memory-conductance:

$$W(\varphi) = b + \frac{a-b}{2}\left(sgn(\varphi+1) - sgn(\varphi-1)\right). \qquad (2)$$

Applying the chain rule to the definition of the current, the expression for i is

$$i = \frac{dq}{dt} = \frac{dq(\varphi)}{d\varphi}\frac{d\varphi}{dt} = W(\varphi)v.$$

Let us define a dimensionless time variable as $\tau = t\bar{t}^{-1}$, where $\bar{t} = C_2 G^{-1}$ stands for the system time scale. The state variables are taken in voltage form as $x_1 = v_1$, $x_2 = v_2$, $x_3 = -G^{-1}i_L$ and $x_4 = \varphi\bar{t}^{-1}$. Introducing dimensionless system parameters $\alpha = C_2C_1^{-1}$, $\beta = C_2L^{-1}G^{-2}$, $\gamma = -G_{N1}G^{-1}$, $\delta = G_{N2}G^{-1}$, $\xi = G^{-1}a$, and $\zeta = G^{-1}b$, the state-space description referring to the oscillator equations is found to be:

$$\begin{aligned}
\frac{dx_1}{d\tau} &= \alpha[-x_3 + \tilde{W}(x_4\bar{t})x_1], \\
\frac{dx_2}{d\tau} &= \gamma x_2 + x_3, \\
\frac{dx_3}{d\tau} &= \beta[x_1 - x_2 - x_3], \\
\frac{dx_4}{d\tau} &= x_1, \qquad (3)
\end{aligned}$$

where, using (2), $\tilde{W}(x_4\bar{t})$ is expressed by

$$\begin{aligned}
\tilde{W}(x_4\bar{t}) &= -\delta - G^{-1}W(x_4\bar{t}) \\
&= \tilde{b} + \frac{\tilde{a}-\tilde{b}}{2}\left(sgn(x_4\bar{t}+1) - sgn(x_4\bar{t}-1)\right), \qquad (4)
\end{aligned}$$

with

$$\tilde{a} = -(\delta+\xi), \qquad (5)$$
$$\tilde{b} = -(\delta+\zeta). \qquad (6)$$

The nonlinearity parameters in (2) are taken as $a = 0.65\,mS$ and $b = 2\,mS$. The system state vector is chosen as $\mathbf{x} = [x_1, x_2, x_3, x_4]' \in \mathbb{R}^4$ with initial condition set to $[0.006, 0.02, -0.3, 0]'$. As for the circuit elements in Fig. 1, we assume the following values: $G = 300^{-1}\,S$, $L = 100\,mH$, $C_1 = 25nF$, $C_2 = 30\,nF$, $G_{N1} = -0.4\,mS$, and $G_{N2} = -0.7\,mS$. As a result, system parameters in (3) are numerically given by $\alpha = 1.2$, $\beta = 0.027$, $\gamma = 0.12$, $\delta = -0.21$, $\xi = 0.195$ $\zeta = 0.6$, $\bar{t} = 9\,us$, $\tilde{a} = 0.0150$ and $\tilde{b} = -0.3900$.

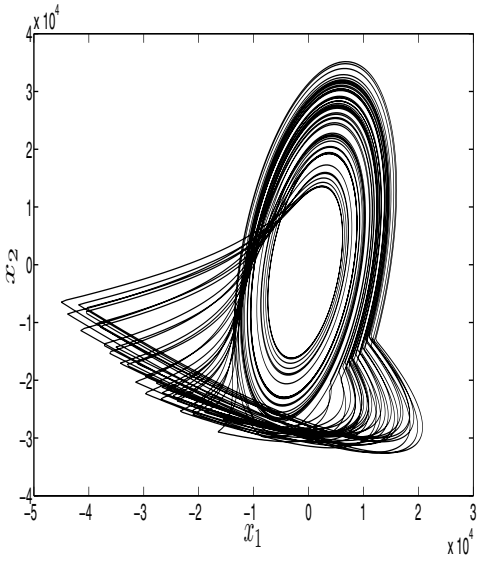

Fig. 2. Plane projection of the chaotic attractor of autonomous system (3) for $\alpha = 1.2$, $\beta = 0.027$, $\gamma = 0.12$, $\delta = -0.21$, $\xi = 0.195$ $\zeta = 0.6$, $\tilde{a} = 0.0150$ and $\tilde{b} = -0.3900$.

As it is demonstrated in Figure 2, where the system attractor is projected on the $x_1 - x_2$ state plane, (3) exhibits chaos under such parameter setting.

The aim of this work is to prove that under particular conditions the theoretical monotone-increasing odd-symmetric charge-flux nonlinearity (1) may be implemented by an appropriate combinations of opposite-polarity memristor nano-scale structures.

In the next Section III we briefly summarize mathematical models of memristor nano-scale structures.

III. Models of memristor nano-scale structures

The memristor nano-structure is a double-layer thin oxide film (e.g. titanium dioxide) with total length D, made up of a conductive layer of oxygen-deficient oxide with length l and of an insulating layer of stoichiometric oxide with length $D - l$. The order of such two layers defines the polarity of the nano-device and is taken into account through coefficient $\eta = \{+1, -1\}$.

The first model of a memristor nano-structure, ascribed to Williams [5], is the combination of a differential equation, governing the time evolution of the length of conductive layer under application of an external source, and of an algebraic equation, referring to the Ohm's based input-output equation. Defining a dimensionless time variable $\tau = t\bar{t}^{-1}$, with $\bar{t}$ denoting the system time scale, Williams' model is expressed by

$$\frac{dx(\tau)}{d\tau} = \eta \ \frac{i(\tau)}{i_0}, \quad (7)$$

$$v(\tau) = (R \circ x)(\tau)\, i(\tau), \quad (8)$$

where $i_0 = \frac{q_0}{t}$, the state variable is taken as $x = lD^{-1}$, $(R \circ x)(\tau)$[1] denotes the memristance or memory-resistance, expressed by

$$\begin{aligned}(R \circ x)(\tau) &= R_{on}x(\tau) + R_{off}\,(1 - x(\tau)) \\ &= R_{off} - \Delta R\ x(\tau), \end{aligned} \quad (9)$$

where $\Delta R = R_{off} - R_{on}$, with R_{on} and R_{off} indicating the memristance of the fully-conductive and of the fully-insulating memristor respectively, while

$$q_0 = \frac{D^2}{\mu R_{on}}$$

is the magnitude of charge required to flow through the device for x to increase from 0 to 1 under a constant external input, with μ standing for the average dopant mobility.

The model, assuming a constant dopant drift rate throughout the entire device length under a constant external input and thus named linear dopant drift model, qualitatively reproduces the dynamics of the memristor with a good degree of accuracy. However, it does not specify boundary conditions. Therefore it is valid only as long as the control source is such that the layer boundary does never reach any end.

Nonlinear dopant drift models ([5],[10],[11]), later introduced to ameliorate the linear model, fall into the following class:

$$\frac{dx(\tau)}{d\tau} = \eta \ \frac{i(\tau)}{i_0}\, F\left(x(\tau), \eta\, i(\tau), p\right), \quad (10)$$

$$v(\tau) = (R \circ x)(\tau) \ \ i(\tau), \quad (11)$$

where $F\left(x, \eta\, i, p\right)$ is a non-negative parameterized (p is a positive integer) window function imposing boundary conditions and possibly accounting for nonlinear effects on ionic transport due to the large electric field developing across the conductive nano-scale layer under application of an external input.

Joglekar [11] proposed a window function F independent on $\eta\, i$ (let us call it F_J):

$$F_J\left(x, p\right) = 1 - \left(2x - 1\right)^{2p}, \quad (12)$$

where p controls the window decrease rate (from the maximum unitary value at $x = 0.5$), occurring as x approaches either 0 or 1. For $p = 1$ (12) is identical (for less than a proportionality factor) to another window previously proposed by Williams himself in [5]. Furthermore, (12) is responsible for the existence of two equilibria, specifically $x = 0$ and $x = 1$, in (10).

[1]Throughout the manuscript the following notation is adopted. For a function $f(\cdot) : \mathbb{R} \to \mathbb{R}$, its argument denotes time whenever it is not explicitly shown. Further, given two functions $f_1(\cdot) : \mathbb{R} \to \mathbb{R}$ and $f_2(\cdot) : \mathbb{R} \to \mathbb{R}$, $(f_1 \circ f_2)\,(\cdot) = f_1(f_2(\cdot)) : \mathbb{R} \to \mathbb{R}$ stands for their composition.

As p gets bigger and bigger, the two x-values at which the window decreases to 90% of its unitary value get farther and farther away from $x = 0.5$ and from those points the window decrease rate becomes larger and larger.

Due to its independence on $\eta\, i$, Joglekar's window may fail to specify realistic boundary conditions. For example it is unable to detect boundary behaviors in the hard-switching scenarios illustrated in plots (a)-(b) of Figure 3 from [5]. By contrast, these dynamics are qualitatively captured by a different window F proposed by Biolek in [10] (let us call it F_B):

$$F_B\left(x, \eta\, i, p\right) = 1 - \left(x - 1\right)^{2p} \ \text{ if } \eta\, i \leq 0, \quad (13)$$

$$F_B\left(x, \eta\, i, p\right) = 1 - x^{2p} \qquad \text{if } \eta\, i > 0. \quad (14)$$

Unlike Joglekar's window, whose unitary maximum is at $x = 0.5$, Biolek's has unitary maxima at $x = 0$ and at $x = 1$. Keeping $\eta = 1$, as p gets bigger and bigger, the x-value at which the window decreases to 90% of its unitary value with $i > 0$ ($i < 0$) gets farther and farther away from $x = 0$ ($x = 1$) and from that point the window decrease rate becomes larger and larger.

One of the main drawbacks of Joglekar's and Biolek's models lies in their inability to capture all the current-voltage characteristics presented in [5] and referring to a memristor nano-structure excited by a sign-varying external input. This modeling inability may be ascribed to the fact that under such kind of external input dynamical system (10)-(11) with window (12) ((13)-(14)) may only exhibit a single-valued (multi-valued) memductance-flux characteristic[2].

A novel model possessing the flexibility to yield both single-valued and multi-valued memductance-flux characteristics under a sign-varying external input is introduced in the next Section. This flexibility is enabled by the fact that the proposed model offers the possibility to tune the boundary conditions according to the specific dynamics under modeling. As a result, this model is named boundary condition-based model (BCM). The versatile nature of the modeled memductance-flux characteristics enables the BCM to replicate all the dynamics reported in [5] with a good level of accuracy. Furthermore, being based upon the linear dopant drift assumption, this model is simple. In fact, unlike Joglekar's and Biolek's models, it possesses closed-form solutions under any input/initial condition combination.

IV. Boundary condition-based model for memristor nano-structures

The BCM consists of the set of differential-algebraic equations (10)-(11) employing the following window F (let us call it $\tilde{F}$):

$$\tilde{F}\left(x(\tau), \eta\, i(\tau)\right) = \begin{cases} 1 & \forall\ \tau\ : C_1 \text{ holds}, \\ 0 & \forall\ \tau\ : C_2 \text{ or } C_3 \text{ holds}, \end{cases} \quad (15)$$

[2]It is worthy to point out that one way to completely define a memristor is by means of its memductance-flux relationship.

where tunable conditions C_m $m = \{1, 2, 3\}$ are defined as

$$C_1 = \{x(\tau) \in (0,1) \mid (x(\tau) = 0 \ \& \ \eta \ i(\tau) > i_{th,0}) \ |(\ x(\tau) = 1 \ \& \ \eta \ i(\tau) < -i_{th,1})\}, \quad (16)$$

$$C_2 = \{x(\tau) = 0 \ \& \ \eta \ i(\tau) \leq i_{th,0}\}, \quad (17)$$

$$C_3 = \{x(\tau) = 1 \ \& \ \eta \ i(\tau) \geq -i_{th,1}\}, \quad (18)$$

where, referring to the case $\eta = +1$ for simplicity, $i_{th,0}$ ($i_{th,1}$) denotes the threshold current the magnitude of the external input needs to pass over after it gets positive (negative) while (17) ((18)) holds, before (16) may be met.

As in Biolek's case, the proposed window depends on the control source. Under sign-varying input, for $x \in (0, 1)$ it may evolve on a single curve only (similarly to Joglekar's case), while for x at boundary $x = 1$ ($x = 0$), it experiences $1 \to 0$ and $0 \to 1$ vertical transitions for $\eta i \geq -i_{th,1}$ and $\eta i < -i_{th,1}$ (for $\eta i \leq i_{th,0}$ and $\eta i < -i_{th,1}$).

The main difference with Biolek's window lies in the fact that ours may only experience vertical transitions when x equals 0 or 1[3]. In fact, in case current sign is reversed while $x \in (0, 1)$, this simply causes state variable to vary in the opposite direction according to (10) (with (15) keeping its unitary value due to the fulfillment to condition (16)) thereafter. In this case, for $\eta = 1$, the window time evolution occurs only along one path.

A. Analysis of the BCM

Let us integrate the proposed model under conditions (16)-(18).

1) Boundary condition C_1: Let us assume that τ_i be the first instant at which condition (16) is fulfilled for the i^{th} instance ($i = \{1, 2, \ldots\}$). Further, let C_1 be the operating condition at the start of the investigation. Let us integrate (10)-(11) with window (15) and under condition (16). Time integrating both sides of (10), state variable x is found to be a function of charge q. Its expression and the corresponding inverse function assume the following forms:

$$(x \circ q)(\tau) = x(\tau_i) + \frac{\eta\,[q(\tau) - q(\tau_i)]}{q_0}, \quad (19)$$

$$(q \circ x)(\tau) = q(\tau_i) + \frac{q_0\,[x(\tau) - x(\tau_i)]}{\eta}, \quad (20)$$

where $q(\tau_i) = \int_{-\infty}^{\tau_i} i(\tau')d\tau'$ designates the entire current history.

From (19) it is evident that the normalized length of conductive layer is a linear function of charge. Thereby, using (20), time-varying values of charge q when $x = 0$ and 1 are respectively expressed by:

$$(q \circ x)(\tau_0) = q(\tau_i) - \frac{q_0}{\eta}\,x(\tau_i) \quad (21)$$

$$(q \circ x)(\tau_1) = q(\tau_i) + \frac{q_0}{\eta}[1 - x(\tau_i)] = (q \circ x)(\tau_0) + \frac{q_0}{\eta}. \quad (22)$$

where τ_0 and τ_1 are such

$$\tau_0 = \{\tau : x(\tau) = 0\} = \bigcup_j \{\alpha_0^{(j)}, \beta_0^{(j)}\}, \quad (23)$$

$$\tau_1 = \{\tau : x(\tau) = 1\} = \bigcup_k \{\alpha_1^{(k)}, \beta_1^{(k)}\}. \quad (24)$$

with $\alpha_0^{(j)}$ ($\alpha_1^{(k)}$) and $\beta_0^{(j)}$ ($\beta_1^{(k)}$) referring to the instant of the j^{th} (k^{th}) ($j, k = \{1, 2, \ldots\}$) occurrence of transition between conditions C_1 and C_2 (C_3) and of the j^{th} (k^{th}) occurrence of transition between conditions C_2 (C_3) and C_1[4].

Remark 1: Note that initial conditions $x(\tau_i)$ and $q(\tau_i)$, depending on the specific i^{th} occurrence of condition C_1 under exam, yield time dependence of (21)-(22) and are at the origin of the multi-valued nature of the charge-flux characteristic arising from the proposed window with boundary conditions (16)-(18) under a generic time-varying external input causing a transition from (to) C_1 to (from) either C_2 or C_3.

Using (10) to express i in terms of $\frac{dx(\tau)}{d\tau}$, inserting such expression into (11), using (9) and time integrating both sides of the resulting equation, the time-dependence of flux φ through state variable x is found to be:

$$(\varphi \circ x)(\tau) = \varphi(\tau_i) + \frac{q_0\,R_{off}}{\eta}[x(\tau) - x(\tau_i)] - \frac{q_0\,\Delta R}{2\,\eta}[x^2(\tau) - x^2(\tau_i)], \quad (25)$$

where $x(\tau_i) = \int_{-\infty}^{\tau_i} dx(\tau')$ and $\varphi(\tau_i) = \int_{-\infty}^{\tau_i} v(\tau')d\tau'$ denote the initial values for normalized length of conductive layer and flux respectively.

From (25) it follows that the time-varying values flux assumes at $x = 0$ and at $x = 1$ are respectively given by:

$$(\varphi \circ x)(\tau_0) = \varphi(\tau_i) - \frac{q_0}{\eta}R_{off}x(\tau_i) + \frac{q_0\Delta R}{2\,\eta}x^2(\tau_i), \quad (26)$$

$$(\varphi \circ x)(\tau_1) = \frac{q_0}{\eta}R_{off}[1 - x(\tau_i)] - \frac{q_0\Delta R}{2\,\eta}[1 - x^2(\tau_i)] + \varphi(\tau_i) = (\varphi \circ x)(\tau_0) + \frac{q_0(R_{off} + R_{on})}{2\,\eta} \quad (27)$$

Note that time variation of (26)-(27) is due to initial conditions $x(\tau_i)$ and $\varphi(\tau_i)$, which, in general, differ according

[3]In one of its forms, particularly in the matched case with $i_{th,0} = i_{th,1} = i_{th} = 0\,A$, (15) is an approximation to Biolek's window for very large p.

[4]Memristor usually operates under periodic control source with period T. As a consequence q, φ and x are periodic with the same period. In such a case, τ_0 and τ_1 assume simpler expressions. For example, assuming that over one period the temporal succession of fulfilled boundary conditions is C_1-C_2-C_1-C_3-C_1, then $\tau_0 = \{\alpha_0 + nT, \beta_0 + nT\}$ and $\tau_1 = \{\alpha_1 + nT, \beta_1 + nT\}$ for $n = 0, 1, 2, \ldots$.

to the particular i^{th} occurrence of C_1. Inserting (19) into (25), the memristor flux-charge mathematical relationship holding under the i^{th} manifestation of condition C_1 is thus obtained:

$$\begin{aligned}(\varphi \circ q)(\tau) &= \varphi(\tau_i) + (R \circ x)(\tau_i)[\, q(\tau) - q(\tau_i)] \\ &\quad -\frac{\eta\,\Delta R}{2\,q_0}[\, q(\tau) - q(\tau_i)]^2, \end{aligned} \tag{28}$$

Inverting (28), the expression for charge in terms of flux under the i^{th} manifestation of C_1 is found to be:

$$\begin{aligned}(q \circ \varphi)(\tau) &= q(\tau_i) + \frac{q_0\,(R \circ x)(\tau_i)}{\eta\,\Delta R} - \frac{q_0\,(R \circ x)(\tau_i)}{\eta\,\Delta R} \\ &\quad \sqrt{1 - \frac{2\,\eta\,\Delta R}{q_0\,[(R \circ x)(\tau_i)]^2}[\varphi(\tau) - \varphi(\tau_i)]}. \end{aligned} \tag{29}$$

Note that flux (charge)-differentiating (29) ((28)) yields the expressions for the memductance (memristance).

2) Boundary condition C_2: Let us consider time interval $\tau \in [\alpha_0^j, \beta_0^j]$, where condition C_2 is fulfilled for the j^{th} instance ($j = \{1, 2, \ldots\}$). Here $\tilde{F}\,(x, \eta\, i) = 0$, therefore, from (10) $x(\tau) = 0$ and $R \circ (x)(\tau) = R_{off}\ \forall\ \tau$ in the given time interval. The φ–q relationship is derived from (11), rewritten as $v(\tau) = R_{off}\, i(\tau)$:

$$\varphi(\tau) = \varphi(\alpha_0^{(j)}) + R_{off}\,[q(\tau) - q(\alpha_0^{(j)})], \tag{30}$$

where $q(\tau) = q(\alpha_0^{(j)}) + \int_{\alpha_0^{(j)}}^{\tau} i(\tau')\, d\tau'$.

Inverting yields the following q-φ relation:

$$q(\tau) = q(\alpha_0^{(j)}) + \frac{\varphi(\tau) - \varphi(\alpha_0^{(j)})}{R_{off}} \tag{31}$$

3) Boundary condition C_3: We then focus on time interval $\tau \in [\alpha_1^k, \beta_1^k]$, where condition C_3 is fulfilled for the k^{th} instance ($k = \{1, 2, \ldots\}$). We have $\tilde{F}\,(x, \eta\, i) = 0$. As a result, (10) yields $x(\tau) = 1$ and $R \circ (x)(\tau) = R_{on}\ \forall\ \tau$ in the given time interval. The φ–q relationship is derived from (11), rewritten as $v(\tau) = R_{on}\, i(\tau)$:

$$\varphi(\tau) = \varphi(\alpha_1^{(k)}) + R_{on}\,[q(\tau) - q(\alpha_1^{(k)})], \tag{32}$$

where $q(\tau) = q(\alpha_1^{(k)}) + \int_{\alpha_1^{(k)}}^{\tau} i(\tau')\, d\tau'$.

Inverting yields the following q-φ relation:

$$q(\tau) = q(\alpha_1^{(k)}) + \frac{\varphi(\tau) - \varphi(\alpha_1^{(k)})}{R_{on}} \tag{33}$$

V. Practical memristors with single-valued q-φ characteristics

From the analysis of Sections IV-A1-IV-A3 it is clear that, due to the time-varying values of (21)-(22) the charge-flux characteristic arising from the proposed window with boundary conditions (16)-(18) under a generic time-varying external input exhibits multi-valuedness. In the next section we shall determine the conditions for a single-valued q-φ relationship.

A. Conditions for a single-valued q-φ relationship

Let us assume that for all $j = 1, 2, \ldots$ the following conditions hold

$$q(\beta_0^{(j)}) = q(\alpha_0^{(j)}) = q_{th0} \quad \Rightarrow \quad \int_{\alpha_0^{(j)}}^{\beta_0^{(j)}} i(\tau)\, d\tau = 0, \tag{34}$$

where (see (21))

$$q_{th0} = (q \circ x)(\alpha_0^{(1)}). \tag{35}$$

Using (IV-A2), conditions (34) imply that for all $j = 1, 2, \ldots$ we also have:

$$\varphi(\beta_0^{(j)}) = \varphi(\alpha_0^{(j)}) = \varphi_{th0} \quad \Rightarrow \quad \int_{\alpha_0^{(j)}}^{\beta_0^{(j)}} v(\tau)\, d\tau = 0 \tag{36}$$

where (see (26))

$$\varphi_{th0} = (\varphi \circ x)(\alpha_0^{(1)}). \tag{37}$$

Similarly, for all $k = 1, 2, \ldots$ we assume that

$$q(\beta_1^{(k)}) = q(\alpha_1^{(k)}) = q_{th1} \quad \Rightarrow \quad \int_{\alpha_1^{(k)}}^{\beta_1^{(k)}} i(\tau)\, d\tau = 0 \tag{38}$$

where (see (22))

$$q_{th1} = (q \circ x)(\alpha_1^{(1)}). \tag{39}$$

Using (IV-A3), from conditions (38) it follows that for all $k = 1, 2, \ldots$

$$\varphi(\beta_1^{(k)}) = \varphi(\alpha_1^{(k)}) = \varphi_{th1} \quad \Rightarrow \quad \int_{\alpha_1^{(k)}}^{\beta_1^{(k)}} v(\tau)\, d\tau = 0 \tag{40}$$

where (see (27))

$$\varphi_{th1} = (\varphi \circ x)(\alpha_1^{(1)}). \tag{41}$$

It turns out (34) and (38) imply equal charge (flux) values at pair of instants $\alpha_0^{(j)}$ and $\beta_0^{(j)}$ ($j = 1, 2, \ldots$) and at pair of instants $\alpha_1^{(k)}$ and $\beta_1^{(k)}$) ($k = 1, 2, \ldots$), i.e. when x leaves and reaches the end 0 (1).

As a result, assuming $\eta = +1$, under condition C_2 (C_3) x halts at 0 (1), while q and φ get smaller (larger) than q_{th0} and φ_{th0} (q_{th1} and φ_{th1}) respectively.

Thereby, under the assumption that (34) and (38) are fulfilled, a novel boundary condition-based window function F (let us called it $\bar{F}$) may be defined:

$$\bar{F}\,(x(\tau), \eta\, i(\tau)) = \begin{cases} 1 & \forall \tau\ : S_1 \text{ holds} \\ 0 & \forall \tau\ : S_2 \text{ or } S_3 \text{holds} \end{cases} \tag{42}$$

where conditions S_k ($k = 1, 2, 3$) are expressed as

$$S_1 = \left\{ x(\tau) \in (0,1) \text{ or } \left(x(\tau) = 0 \text{ and } \eta \int_{-\infty}^{\tau} i(\tau')d\tau' > \eta\, q_{th0} \right) \right. \\ \left. \text{or } \eta \left(x(\tau) = 1 \text{ and } \int_{-\infty}^{\tau} i(\tau')d\tau' < \eta\, q_{th1} \right) \right\}, \quad (43)$$

$$S_2 = \left\{ x(\tau) = 0 \text{ and } \eta \int_{-\infty}^{\tau} i(\tau')d\tau' \leq \eta\, q_{th0} \right\}, \quad (44)$$

$$S_3 = \left\{ x(\tau) = 1 \text{ and } \eta \int_{-\infty}^{\tau} i(\tau')d\tau' \geq \eta\, q_{th1} \right\}. \quad (45)$$

Throughout the remaining part of this work the model adopted for the memristor is (10)–(11) with window (42). This model exhibits a single-valued q-φ relationship, analytically derived in the next Section.

B. Model integration

Let us assume that τ_i be the first instant at which condition S_1 is fulfilled for the i^{th} instance ($i = \{1, 2, \ldots\}$). Let S_1 be the fulfilled condition at the start of the investigation. Proceeding as in Section IV-A1, under the i^{th} occurrence of S_1 ($i = \{1, 2, \ldots\}$) the charge-flux relation is expressed by (29), where the intervals of allowable values for q and φ respectively are $\eta\ q \in \eta\ [q_{th0}, q_{th1}]$ and $\eta\ \varphi \in \eta\ [\varphi_{th0}, \varphi_{th1}]$.

Let us now consider time interval $\tau \in [\alpha_0^j, \beta_0^j]$, where condition S_2 is fulfilled for the j^{th} instance ($j = \{1, 2, \ldots\}$). Referring to Section IV-A2, the q-φ relation is given by (31), where $q(\alpha_0^{(j)}) = q_{th0}$ and $\varphi(\alpha_0^{(j)}) = \varphi_{th0}$. Note that here the intervals of allowable values for q and φ respectively are $\eta\ q \in \eta\ (-\infty, q_{th0}]$ and $\eta\ \varphi \in \eta\ (-\infty, \varphi_{th0}]$.

Finally, let us focus on the k^{th} instance of condition S_3 ($k = \{1, 2, \ldots\}$), occurring over time interval $\tau \in [\alpha_0^k, \beta_0^k]$. Recalling Section IV-A3, the q-φ relation is expressed by (33), with $q(\alpha_1^{(k)}) = q_{th1}$ and $\varphi(\alpha_1^{(k)}) = \varphi_{th1}$. In this case intervals of allowable values for q and φ respectively are $\eta\ q \in \eta\ [q_{th1}, \infty)$ and $\eta\ \varphi \in \eta\ [\varphi_{th1}, \infty)$.

As a result, the expression for charge in terms of flux is finally expressed by

$$(q \circ \varphi)(\tau) = \begin{cases} q(\tau_i) + \frac{q_0\,(R \circ x)(\tau_i)}{\eta\,\Delta R} - \frac{q_0\,(R \circ x)(\tau_i)}{\eta\,\Delta R} \\ \sqrt{1 - \frac{2\,\eta\,\Delta R}{q_0\,[(R \circ x)(\tau_i)]^2}[\varphi(\tau) - \varphi(\tau_i)]} & \text{if } S_1 \text{ holds}, \\ q_{th0} + \frac{\varphi(\tau) - \varphi_{th0}}{R_{off}} & \text{if } S_2 \text{ holds}, \\ q_{th1} + \frac{\varphi(\tau) - \varphi_{th1}}{R_{on}} & \text{if } S_3 \text{ holds}. \end{cases} \quad (46)$$

The flux-charge mathematical relationship may be obtained by using (28), (IV-A3) and (IV-A2).

Let us consider an exemplifying numerical example. For simplicity, we assume that $x(\tau_i) = 0$ (implying $(R \circ x)(\tau_i) = R_{off}$), $q(\tau_i) = 0$ and $\varphi(\tau_i) = 0$ at the start of the investigation, that is at instance $i = 1$ of condition S_1. From (35) and (21) it follows that $q_{th0} = (q \circ x)(\alpha_0^1) = 0$, while (39) and (22) gives $q_{th1} = (q \circ x)(\alpha_1^1) = \eta\, q_0$. Using first pair of equations (37) and (26) and then pair of equations (41) and (27) we then have:

$$\varphi_{th0} = (\varphi \circ x)(\alpha_0^1) = 0 \quad (47)$$

$$\varphi_{th1} = (\varphi \circ x)(\alpha_1^1) = \frac{q_0}{2\eta}(R_{off} + R_{on}). \quad (48)$$

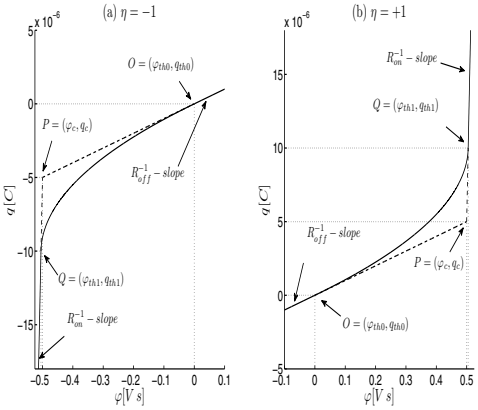

Fig. 3. Memristor q-φ nonlinearity (solid curve) and its PWL approximation (linear parts of the solid curve and their dashed line extensions) with η set to -1 (plot(a)) and $+1$ (plot(b)).

As for the parameter setting, we select typical values reported in [11]: $D = 10\ nm$, $\mu = 10^{-14}\frac{m^2}{Vs}$ and $R_{off} = 100\, R_{on}$. Choosing $R_{on} = 1\,k\Omega$ implies $R_{off} = 100\,k\Omega$, $\Delta R = 99\,k\Omega$ and $q_0 = 10^{-5}\,C$. From (47)–(48) it follows that $\varphi_{th0} = 0\,Vs$, and $\varphi_{th1} = \pm\ 0.505\,Vs$ (the positive sign refers to $\eta = +1$).

Figures $3(a)$–$3(b)$ respectively depict the single-valued q-φ characteristic, as it is mathematically given in (46), for $\eta = -1$ and for $\eta = +1$ (solid curves). In each of these plots the linear parts of the solid curve and their dashed-line extensions determine the two-half-line-based PWL approximation to (46).

The simple PWL approximation to (46), often adopted in literature [7], consists of the tangent lines to the function defined by (46) at points $O = (\varphi_{th0}, q_{th0})$ and $Q = (\varphi_{th1}, q_{th1})$. These lines, expressed by (33) with $q(\alpha_1^{(k)}) = q_{th1}$ and $\varphi(\alpha_1^{(k)}) = \varphi_{th1}$ and by (31) with $q(\alpha_0^{(j)}) = q_{th0}$ and $\varphi(\alpha_0^{(j)}) = \varphi_{th0}$, have angular coefficients respectively equal to R_{on}^{-1} and R_{off}^{-1} and meet at point $P = (\varphi_c, q_c)$, whose coordinates may be expressed in the following form:

$$\varphi_c = \frac{q_0}{2\,\eta} R_{off}, \quad (49)$$

$$q_c = \frac{q_0}{2\,\eta}. \quad (50)$$

In the numerical example the angular coefficients of the PWL approximation to (46) respectively equal $R_{on}^{-1} = 10^{-3}\,S$ and $R_{off}^{-1} = 10^{-5}\,S$. Using (49) and (50), the coordinates of the non-differentiability point of the PWL approximation to (46) are $\varphi_c = \pm\ 0.5\,Vs$ and $q_c = \pm 0.5\ 10^{-5} C$ (the positive sign for both φ_c and q_c is associated to $\eta = +1$).

VI. Combination of memristor nano-structures with symmetrical charge-flux nonlinearity

Although the single-valued q-φ relation expressed by (46) is asymmetric, complementary behaviors arise in memristors with opposite polarity (see plots (a)-(b) in Figure 3). Thus it may be demonstrated that the theoretical monotone-increasing

odd-symmetric charge-flux nonlinearity (1), suitable for chaos-based applications, may be implemented through a suitable interconnection of these kinds of memristors, specifically the anti-parallel arrangement.

The following constraints, due to Kirchhoff's Voltage and Current Laws, link charge and flux variables of memristors m_1 and m_2 at any time:

$$q = q_1 + q_2, \tag{51}$$
$$\varphi = \varphi_1 = \varphi_2, \tag{52}$$

where q_1 and q_2 (φ_1 and φ_2) denote the charge through (flux across) m_1 and m_2 respectively, while q and φ respectively stand for charge and flux of the passive bipole resulting from their combination.

Using (51)-(52), the q-φ relation for the anti-parallel arrangement may in general feature $3 \cdot 3$ different expressions, i.e. as many different expressions as the number of possible combinations of conditions $S_{j,m}$ (m=$\{1,2,3\}$) for the two memristors m_j ($j = \{1, 2\}$). However we are interested in a simpler case. In fact we assume identical memristors, i.e. we set $D_j = D$, $\mu_j = \mu$, $R_{j,on} = R_{on}$ and $R_{j,off} = R_{off}$. This implies $\Delta R_j = R_{j,off} - R_{j,on} = \Delta R$ and $q_{j,0} = \frac{D_j^2}{\mu_j R_{j,on}} = q_0$. Let us assume that $\eta_2 = -\eta_1 = \eta$ with η set to $+1$.

We further assume that at the start of the investigation $S_{j,1}$ is the fulfilled condition for memristor m_j and that $x_j(\tau_i) = 0$ (yielding $(R_j \circ x_j)(\tau_i) = R_{off}$), $q_j(\tau_i) = 0$ and $\varphi_j(\tau_i) = 0$.

Taking (21)-(22) and (47)-(48) into account, it is derived

$$q_{2,th0} = q_{1,th0} = 0,$$

$$q_{2,th1} = -q_{1,th1} = q_0,$$

$$\varphi_{2,th0} = \varphi_{1,th0} = 0,$$

$$\varphi_{2,th1} = -\varphi_{1,th1} = \frac{q_0}{2}(R_{on} + R_{off}).$$

After a number of algebraic calculations the combined memristive element is found to be characterized by the following charge q-flux φ relationship:

$$q(\varphi) = \begin{cases} \varphi(\frac{1}{R_{off}} + \frac{1}{R_{on}}) + \frac{\Delta R}{R_{on}} \frac{q_0}{2\eta} & \forall \varphi \in (-\infty, \varphi_{1,th1}], \\ -\frac{q_0 R_{off}}{\eta \Delta R} + \frac{\varphi}{R_{off}} & \\ +\frac{q_0 R_{off}}{\eta \Delta R} \sqrt{1 + \frac{2\eta \Delta R}{q_0 R_{off}^2} \varphi} & \forall \varphi \in [\varphi_{1,th1}, \varphi_{1,th0}], \\ \frac{q_0 R_{off}}{\eta \Delta R} + \frac{\varphi}{R_{off}} & \\ -\frac{q_0 R_{off}}{\eta \Delta R} \sqrt{1 - \frac{2\eta \Delta R}{q_0 R_{off}^2} \varphi} & \forall \varphi \in [\varphi_{2,th0}, \varphi_{2,th1}], \\ \varphi(\frac{1}{R_{off}} + \frac{1}{R_{on}}) - \frac{\Delta R}{R_{on}} \frac{q_0}{2\eta} & \forall \varphi \in [\varphi_{2,th1}, +\infty). \end{cases} \tag{53}$$

The charge-flux characteristic described by (53) is depicted in Figure 4 (solid curve), where after some algebraic calculations the coordinates of points O, Q_- (here condition $S_{2,2}$ is the fulfilled condition for m_2) and Q_+ (here $S_{1,2}$ is the fulfilled condition for m_1) are found to be:

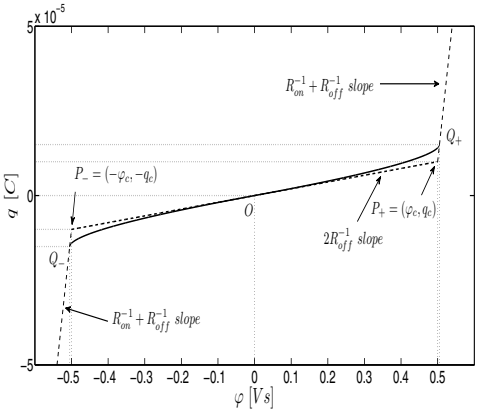

Fig. 4. Charge-flux characteristic (solid curve) and their PWL approximations (linear parts of the solid curves and their dashed-line extensions) for anti-parallel combination of two memristors of Figure 6.

$$\begin{aligned} O &= (\varphi_{1,th0}, q_{1,th0} + q_{2,th0}) = (0, 0), \\ Q_- &= (\varphi_{1,th1}, q_{1,th1} + (q_2(\varphi_{1,th1})) \\ &= \left(-\frac{q_0}{2\eta}(R_{on} + R_{off}), -\frac{q_0}{2\eta} \frac{R_{on} + 3R_{off}}{R_{off}} \right), \\ Q_+ &= (\varphi_{2,th1}, q_{2,th1} + (q_1(\varphi_{2,th1})) = -Q_+, \end{aligned}$$

It may be proved that the PWL approximation to (53) has the same expression as in (1) with

$$a = \frac{2}{R_{off}}, \tag{54}$$
$$b = \frac{1}{R_{off}} + \frac{1}{R_{on}}, \tag{55}$$
$$\varphi_c = \varphi_{2,c} = \frac{R_{off} q_0}{2\eta}. \tag{56}$$

The PWL charge-flux characteristic for the anti-parallel combination is also depicted in Figure 4 (linear parts of the continuous characteristic and their dashed-line extensions), where $P_+ = (\varphi_c, q_c)$ and $P_- = -P_+$ with φ_c expressed by (56) and $q_c = q_{2,c} + (-q_{1,c}) = \frac{q_0}{\eta}$.

We have thus demonstrated that under particular conditions the anti-parallel combination of two memristors permits the electronic implementation of a monotone-increasing odd-symmetric charge-flux nonlinearity suitable for chaos-based applications.

VII. Chaotic neural circuit with practical memristors

The dynamics of an artificially-conceived memristor characterized by symmetric charge-flux characteristic are replicated by a suitable arrangement of practical memristors. In particular, the chaotic behaviors experienced by the original neural circuit of Figure 1 and by its variant employing an anti-parallel combination of identical memristor nano-structures in place of a theoretical memristor with charge-flux nonlinearity (1) (see Figure 5) are equivalent.

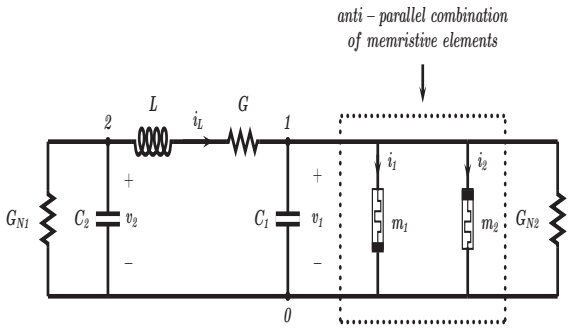

Fig. 5. Variant of the neural oscillator of Figure 1 employing an anti-parallel combination of identical memristor nano-structures –see Figure **??**– in place of the theoretical memristor with charge-flux nonlinearity (1).

We assume that memristor m_j ($j = \{1, 2\}$) has polarity coefficient η_j), length of conductive layer l_j, current $i_j = v_1 R_{mj}^{-1}(l_j D^{-1})$ and memristance $R_{mj}(l_j D^{-1}) = R_{off} - \Delta R l_j D^{-1}$. Let q_0 have the significance outlined in Section III and $\tilde{F}(\cdot, \cdot)$ be the window function defined by (42). With reference to the symbols of Figure 5, applying Circuit Theory laws to this oscillator permits the derivation of its equations.

System state variables are chosen as $x_1 = v_1$, $x_2 = v_2$, $x_3 = -G^{-1} i_L$, $x_4 = l_1 D^{-1}$ and $x_5 = l_2 D^{-1}$. Dimensionless system parameters α, β, γ and δ have the same expressions as in Section II. Introducing dimensionless time variable $\tau = t\bar{t}^{-1}$, with system time scale defined as in Section II, the system state equations referring to the oscillator equations are found to be:

$$\begin{aligned}
\frac{dx_1}{d\tau} &= \alpha \left[-x_3 - \delta x_1 - \tilde{R}_{m1}^{-1}(x_4) x_1 - \tilde{R}_{m2}^{-1}(x_5) x_1 \right], \\
\frac{dx_2}{d\tau} &= \gamma x_2 + x_3, \\
\frac{dx_3}{d\tau} &= \beta [x_1 - x_2 - x_3], \\
\frac{dx_4}{d\tau} &= \eta_1 i_0^{-1} x_1 R_{m1}^{-1}(x_4) \tilde{F}\left(x_4, \eta_1 R_{m1}^{-1}(x_4) x_1\right), \\
\frac{dx_5}{d\tau} &= \eta_2 i_0^{-1} x_1 R_{m2}^{-1}(x_5) \tilde{F}\left(x_5, \eta_2 R_{m2}^{-1}(x_5) x_1\right), \qquad (57)
\end{aligned}$$

where $i_0 = q_0 \bar{t}^{-1}$, $R_{m1}(x_4) = R_{off} - \Delta R x_4$, $R_{m2}(x_5) = R_{off} - \Delta R x_5$, $\tilde{R}_{m1}(x_4) = \rho - \sigma x_4$ and $\tilde{R}_{m2}(x_5) = \rho - \sigma x_5$, with $\rho = G R_{off}$ and $\sigma = G \Delta R$.

Values for circuit parameters G, G_{N1}, G_{N2}, C_1, C_2 and L are set as in Section II. Therefore system parameters in (57), i.e. α, β, γ and δ, are numerically equivalent to the values reported in the caption of Figure 2.

Referring to Section V, the anti-parallel combination of memristor nano-structures is equivalent to the theoretical memristor with odd-symmetric q-φ nonlinearity (1) with the provision that R_{on} and R_{off} are taken as

$$R_{off} = \frac{2}{a}, \qquad (58)$$

$$R_{on} = \frac{2}{2b - a}, \qquad (59)$$

where we made use of (54)-(55). Keeping for a and b the same values chosen in Section II, from (58)-(59) it follows that $R_{off} = 3.077 k\Omega$ and $R_{on} = 0.597\, k\Omega$. As a result $\rho = 10.26$ and $\sigma = 8.27$. Further numerical values for μ and D are kept as it was specified in Section III. Setting $\eta_1 = 1$ and $\eta_2 = -1$, autonomous system (57) exhibits chaotic behavior when initial condition for state vector $\mathbf{x} = [x_1, x_2, x_3, x_4, x_5]' \in \mathbb{R}^5$ is taken as $[0.006,\ 0.02,\ -0.3,\ 0,\ 0]'$. It may be shown that the projection of the system attractor on the x_1-x_2 plane qualitatively and quantitatively agree with Figure 2. This demonstrates that neural circuits in Figures 1 and 5 exhibit equivalent chaotic dynamics.

VIII. Conclusion

Memristor-based chaotic neural networks are able to reproduce complex brain functionalities (learning, associative memory, pattern recognition) leveraging on the chaotic dynamics of real neurons. A theoretical memristor with symmetric charge-flux relation is extensively used in neural networks. We recently introduced a novel boundary condition-based model for practical memristor nano-structures. In this paper we analytically derive the conditions under which an appropriate combination of such nano-structures dynamically acts as the theoretical memristor. The mathematical treatment is validated through numerical simulations on a chaotic neural circuit.

Acknowledgment

This work was partially supported by the *CRT Foundation*, under the project no. 2009.0570, by the Istituto Superiore Mario Boella and the regional government of Piedmont.

References

[1] K. Aihara, T. Takabe, and M. Toyoda, "Chaotic neural networks," *Phys. Lett. A*, vol. 144, pp. 333-340, 1990.

[2] M. Adachi, and K. Aihara, "Associative dynamics in a chaotic neural network," *Neural Networks*, vol. 10, pp. 83-98, 1997.

[3] W. J. Freeman, "Model of biological pattern recognition with spatially chaotic dynamics," *Neural Networks*, vol. 3, pp. 153-170, 1990.

[4] L. O. Chua, "Memristor: the missing circuit element," *IEEE Trans. on Circuit Theory*, vol. 18, no. 5, pp. 507-519, 1971.

[5] D. B. Strukov, G. S. Snider, D. R. Stewart, and R. S. Williams, "The missing memristor found," *Nature*, vol. 453, pp. 80-83, 2008.

[6] Ch. K. Volos, I. M. Kyprianidis, and I. N. Stouboulos "Memristors: a new approach in nonlinear circuits design," *Proc. of the* 14^{th} *WSEAS Int. Conf. on Communication*, pp. 25-30, 2010

[7] M. Itoh, and L. Chua, "Memristor oscillators," *Int. J. Bif. and Chaos*, vol. 18, pp. 3183-3206, 2008.

[8] F. Corinto, A. Ascoli and M. Gilli, "Modeling Dynamics of memristive Nano-Structures," accepted for future publication on the *Proc. of Int. Symp. on Circuits and Systems*, 2012.

[9] M. P. Kennedy, "Three steps to chaos - part II: a Chua's circuit primer," *IEEE Trans. on Circuits and Systems-I*, vol. 40, no. 10, pp. 657-674, Oct. 1993.

[10] Z. Biolek, D. Biolek, and B. Biolková, "Spice model of memristor with nonlinear dopant drift," *Radio Engineering*, vol. 18, no. 2, pp. 210-214, 2009.

[11] Y. N. Joglekar and S. T. Wolf, "The elusive memristor: properties of basic electrical circuits," *Eur. J. Phys.*, vol. 30, pp. 661-675, 2009.